

Figure 2.3.9-23. Normalized Tracer Responses in the Bullfrog Tuff Multiple-Tracer Tests

NOTE: Tracer recoveries were about 69% for pentafluorobenzoic acid (PFBA), 69% for bromide, 39% for lithium, and 15% for microspheres. Concentrations are normalized to mass injected. Tests were conducted between October 1996 and September 1997.

Source: SNL 2007b, Figures D-19 and D-20.

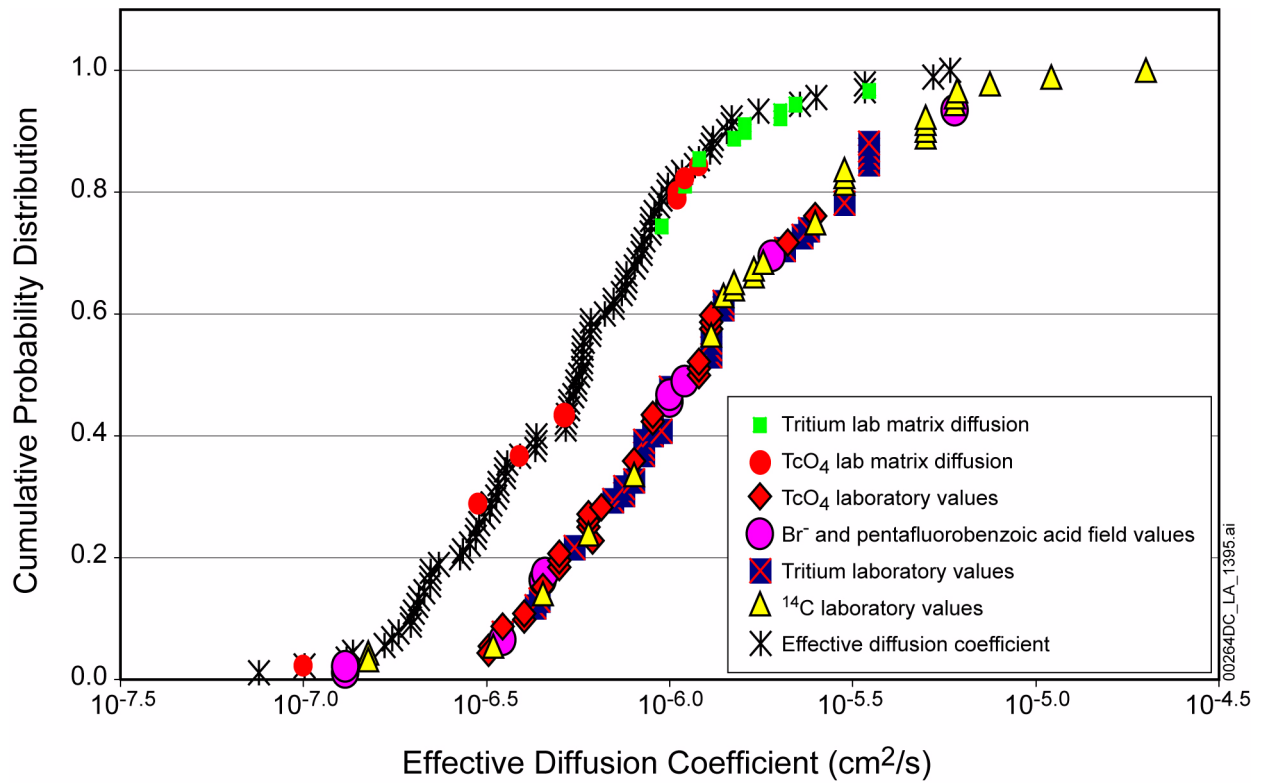


Figure 2.3.9-24. Cumulative Probability Distribution for Matrix Diffusion Coefficients Applicable to Fractured Tuffs at Yucca Mountain

NOTE: The left curve represents effective diffusion coefficient values derived using a linear regression relationship based on porosity and permeability values and diffusion cell results. The right curve represents laboratory and field-derived estimates.

Source: SNL 2008b, Figure 6-14.

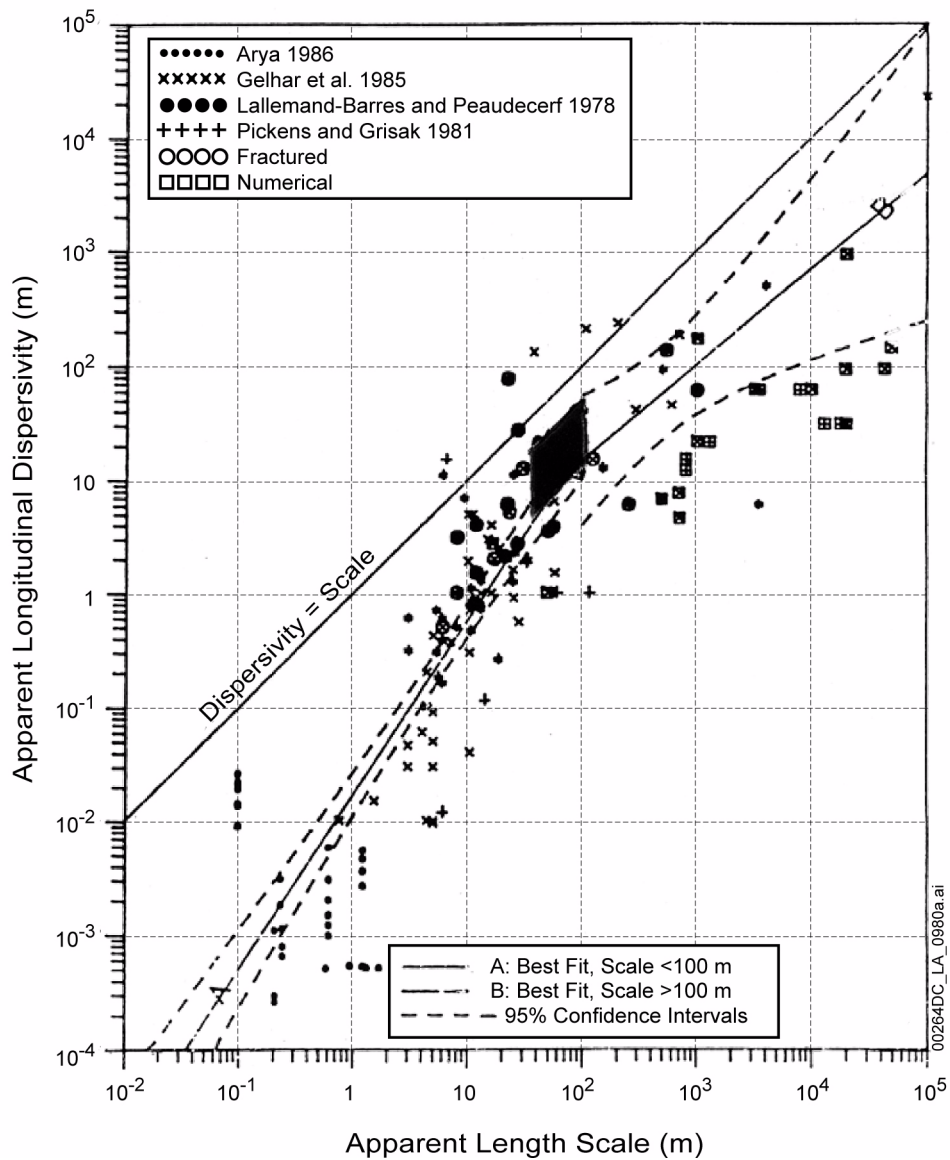


Figure 2.3.9-25. Dispersivity as a Function of Length Scale

NOTE: The darkened box shows the range of values derived from the multiple-tracer field tests at the C-Wells. The right edge of the box corresponds to the interwell separation distance, and the left edge of the box corresponds to the test interval thickness (taken to be the upper limit of transport distance).

Source: SNL 2007b, Figure E-40; Plot taken from Neuman 1990, Figure 1.

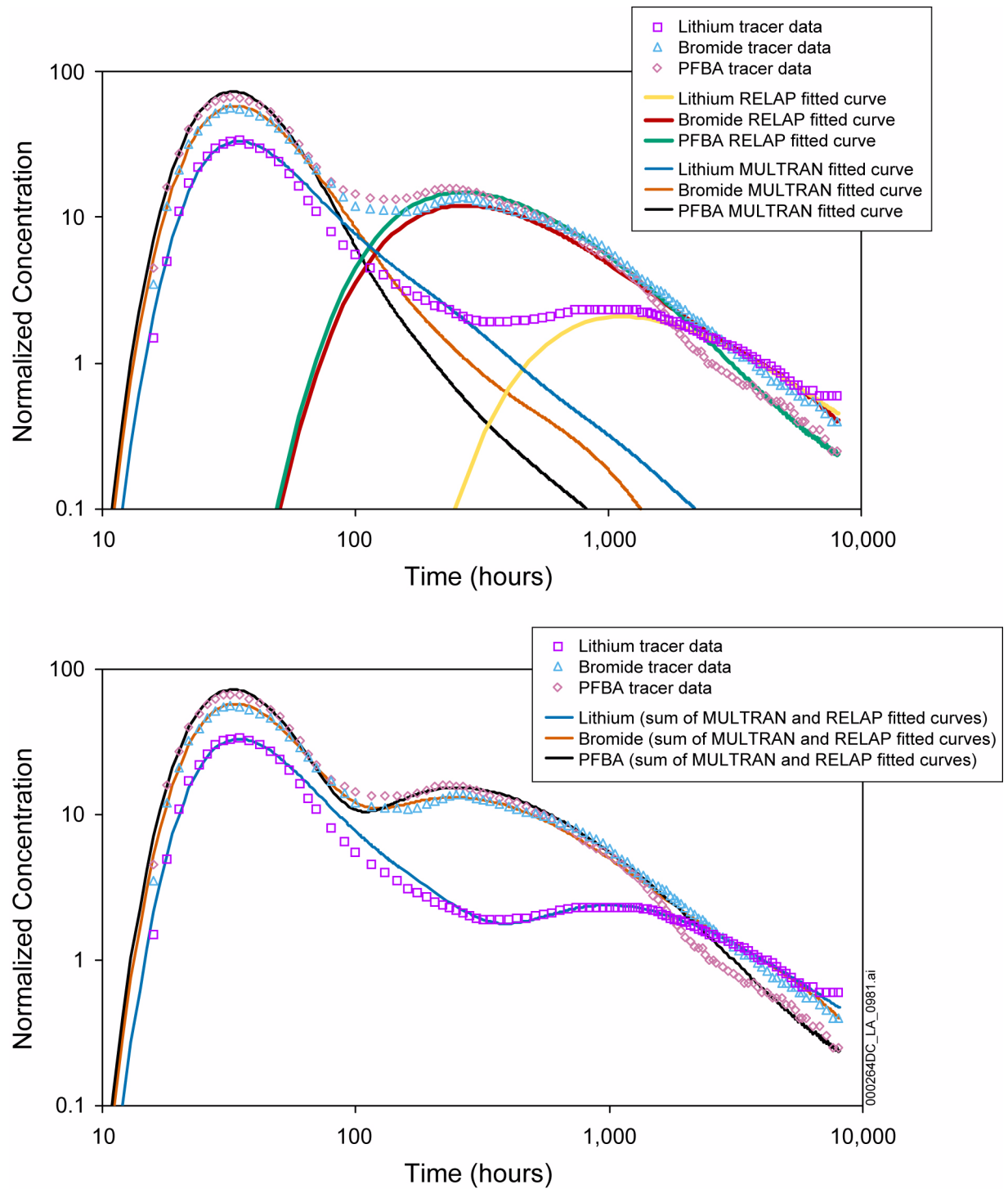


Figure 2.3.9-26. Comparison of Tracer Test Results and Model-Simulated Results at the C-Wells Complex

NOTE: The upper plot shows individual fits to first and second tracer peaks (MULTRAN and RELAP, respectively). The lower plots show composite fits. For clarity, the data points shown are a subset of the actual data.

Source: SNL 2007b, Figure D-26.

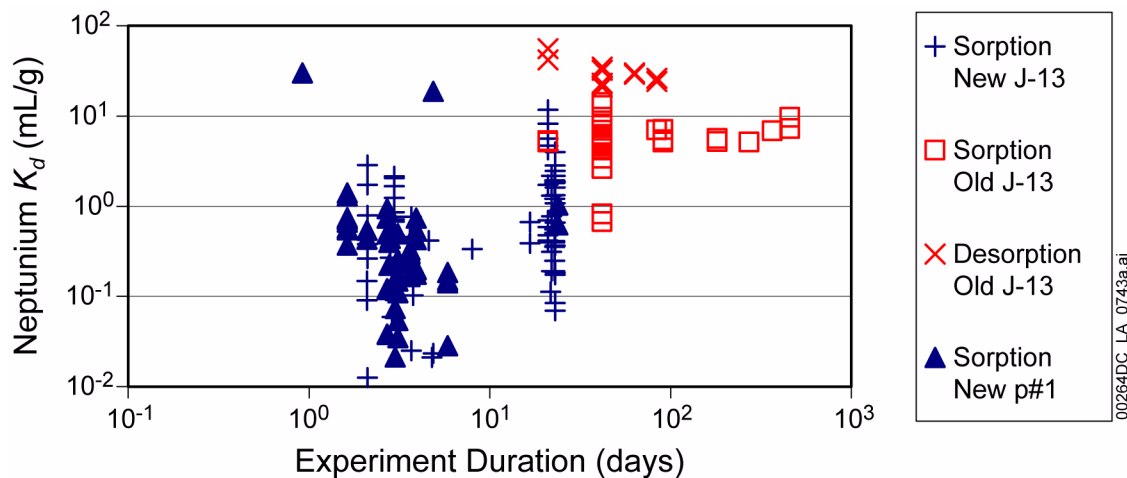


Figure 2.3.9-27. Neptunium Sorption Coefficients on Devitrified Tuff versus Experiment Duration for Sorption and Desorption Experiments

NOTE: Experiments oversaturated with Np_2O_5 have been omitted.

Source: SNL 2008a, Figure A-16.

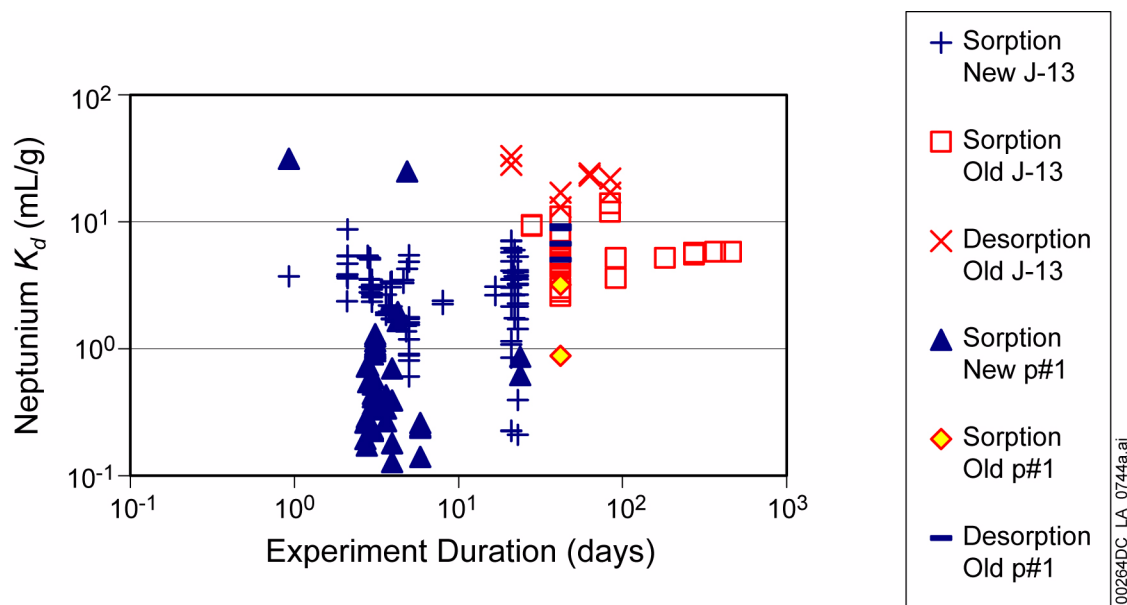


Figure 2.3.9-28. Neptunium Sorption Coefficients on Zeolitic Tuff versus Experiment Duration for Sorption and Desorption Experiments

NOTE: Oversaturated experiments have been omitted.

Source: SNL 2008a, Figure A-19.

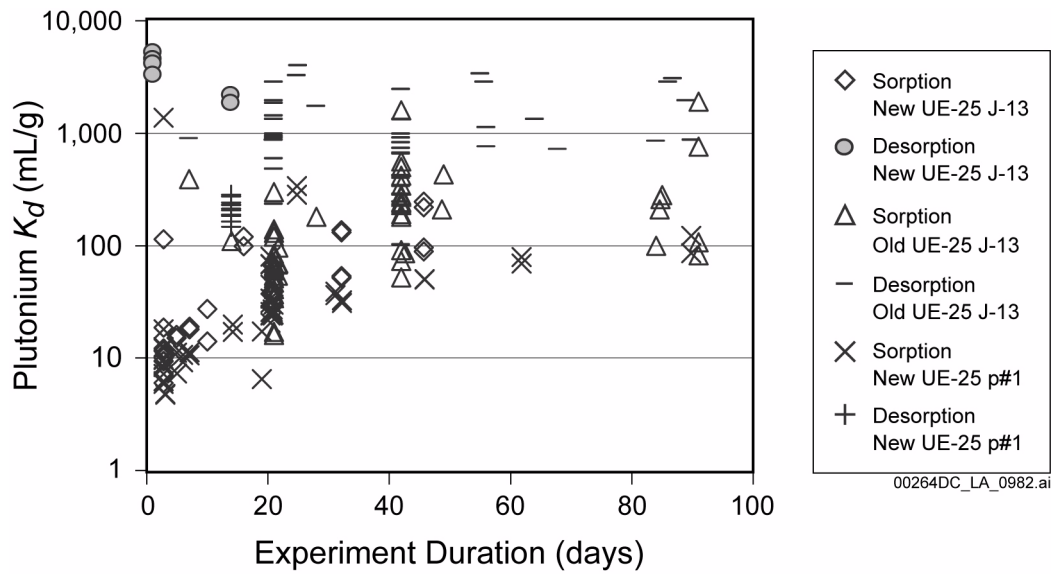


Figure 2.3.9-29. Plutonium Sorption Coefficients on Devitrified Tuff versus Experiment Duration for Sorption and Desorption Experiments

Source: SNL 2008a, Figure A-23.

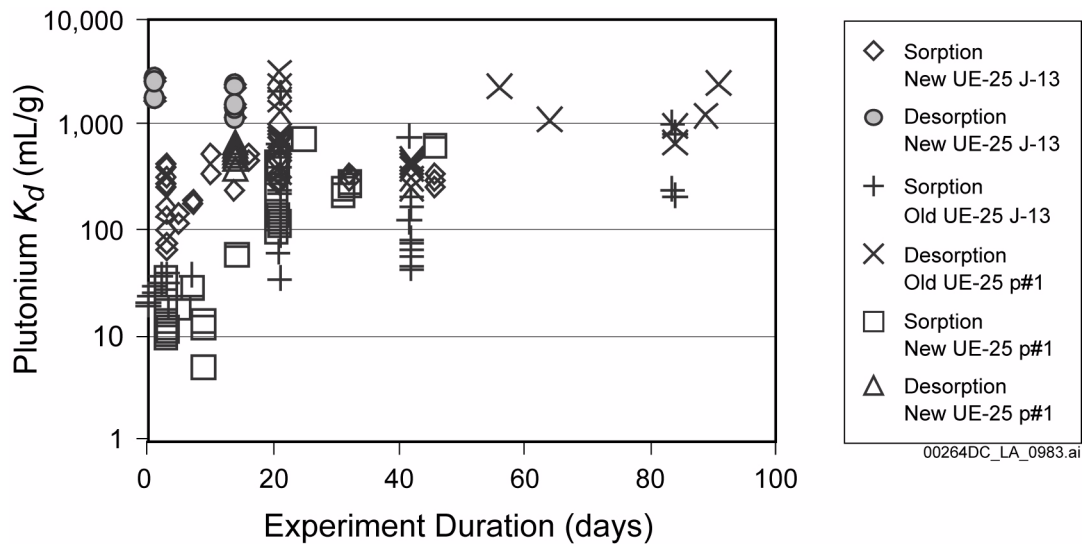


Figure 2.3.9-30. Plutonium Sorption Coefficients on Zeolitic Tuff versus Experiment Duration for Sorption and Desorption Experiments

Source: SNL 2008a, Figure A-27.

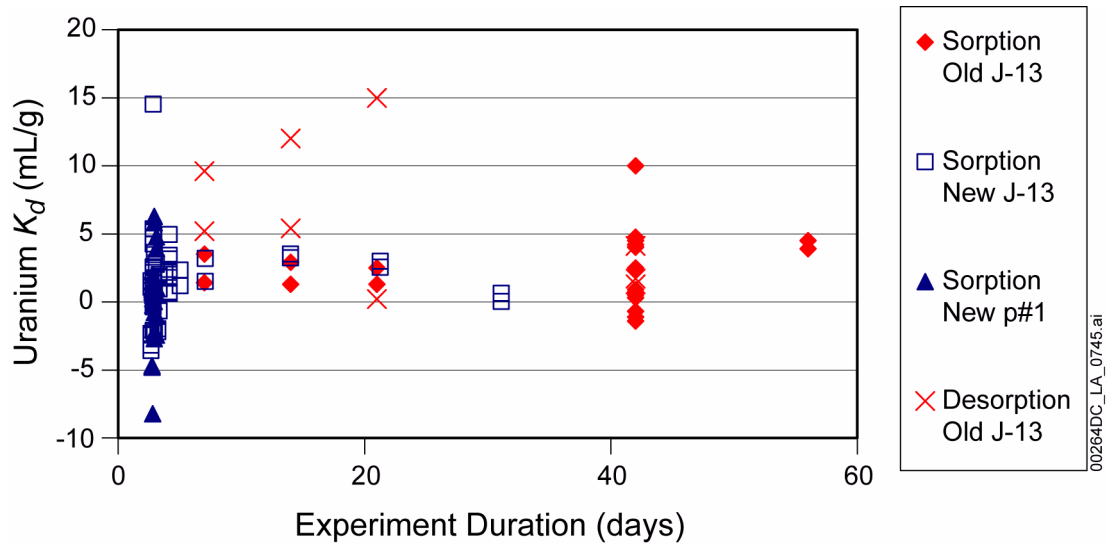


Figure 2.3.9-31. Uranium Sorption Coefficients on Devitrified Tuff versus Experiment Duration for Sorption and Desorption Experiments

Source: SNL 2008a, Figure A-54.

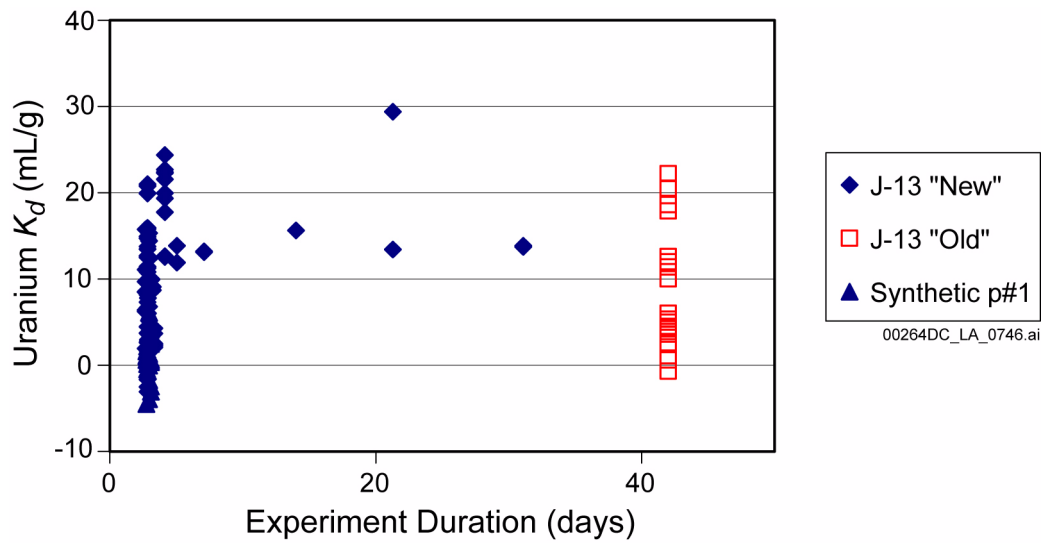


Figure 2.3.9-32. Uranium Sorption Coefficients on Zeolitic Tuff as a Function of Experiment Duration

Source: Adapted from SNL 2008a, Figure A-58.

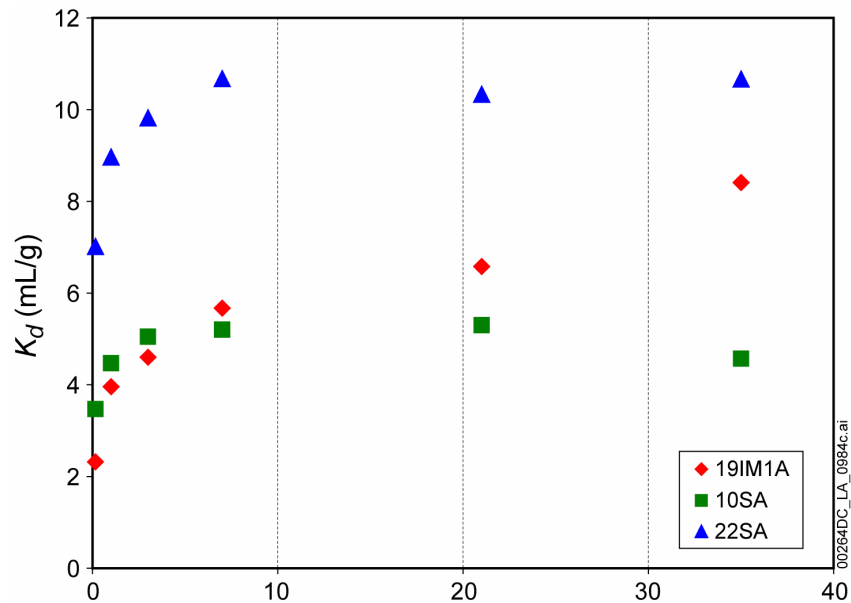


Figure 2.3.9-33. Sorption of ^{233}U onto Alluvium as a Function of Time from Batch Sorption Tests

NOTE: Borehole names refer to Nye County Early Warning Drilling Program boreholes. Groundwater from well NC-EWDP-19D, Zone 1, was used in the experiments for samples -19IM1A and -22SA. Groundwater from well NC-EWDP-10S was used in the experiment for sample -10SA.

Source: SNL 2008a, Figure G-9.

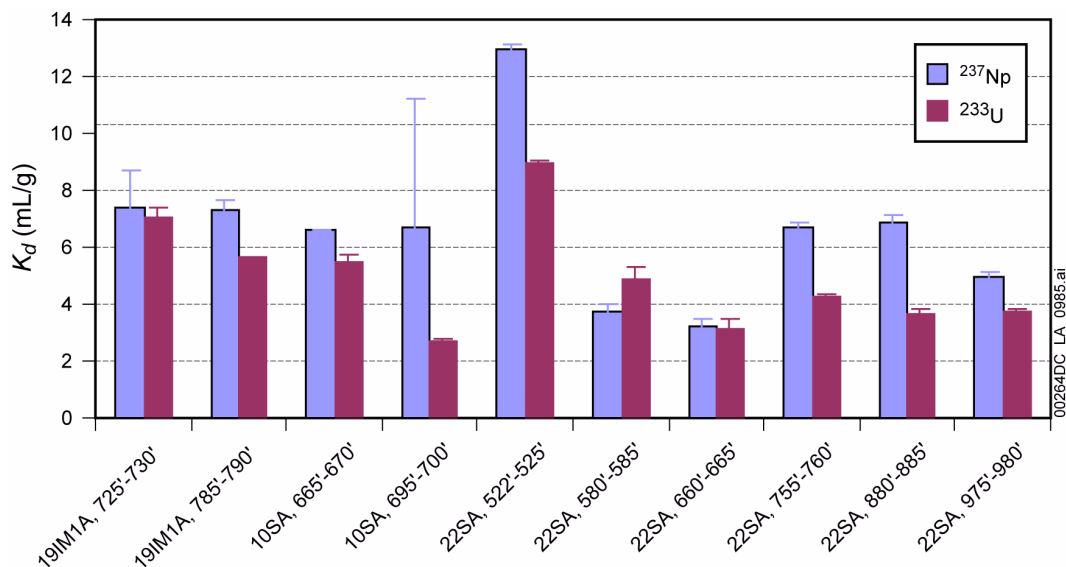


Figure 2.3.9-34. Sorption Coefficients of ^{237}Np and ^{233}U in Alluvium from Batch Sorption Tests

NOTE: Borehole names refer to Nye County Early Warning Drilling Program boreholes. Groundwater from well NC-EWDP-19D, Zone 1, was used in the experiments for samples -19IM1A and -22SA. Groundwater from well NC-EWDP-10S was used in the experiment for sample -10SA.

Source: SNL 2008a, Figure G-7.

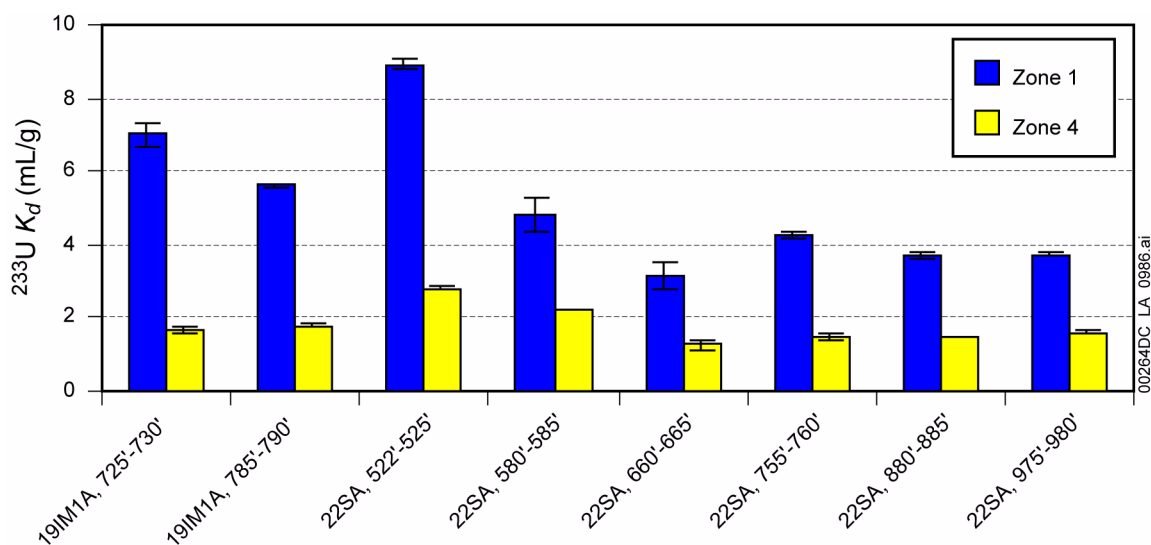


Figure 2.3.9-35. Sorption of ^{233}U in Borehole NC-EWDP-19D Zone 1 and Zone 4 Waters from Batch Sorption Tests

NOTE: Borehole names refer to Nye County Early Warning Drilling Program boreholes.

Source: SNL 2008a, Figure G-8.

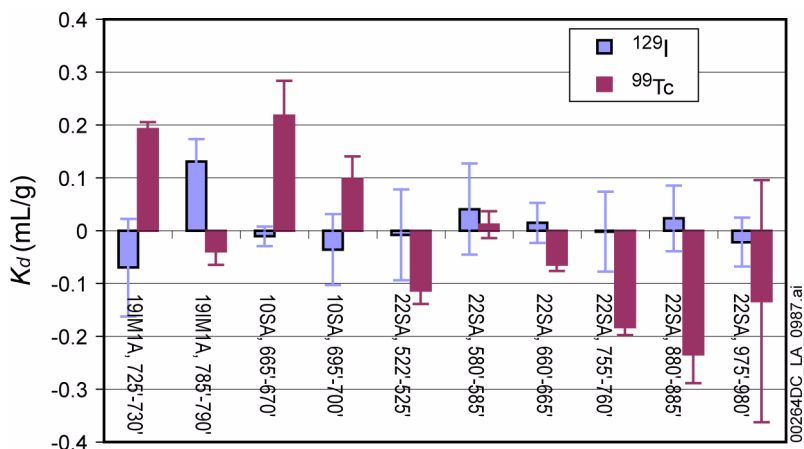


Figure 2.3.9-36. Sorption Coefficients of ^{129}I and ^{99}Tc in Alluvium from Laboratory Column Transport Experiments

NOTE: Borehole names refer to Nye County Early Warning Drilling Program boreholes.

Source: SNL 2008a, Figure G-6.

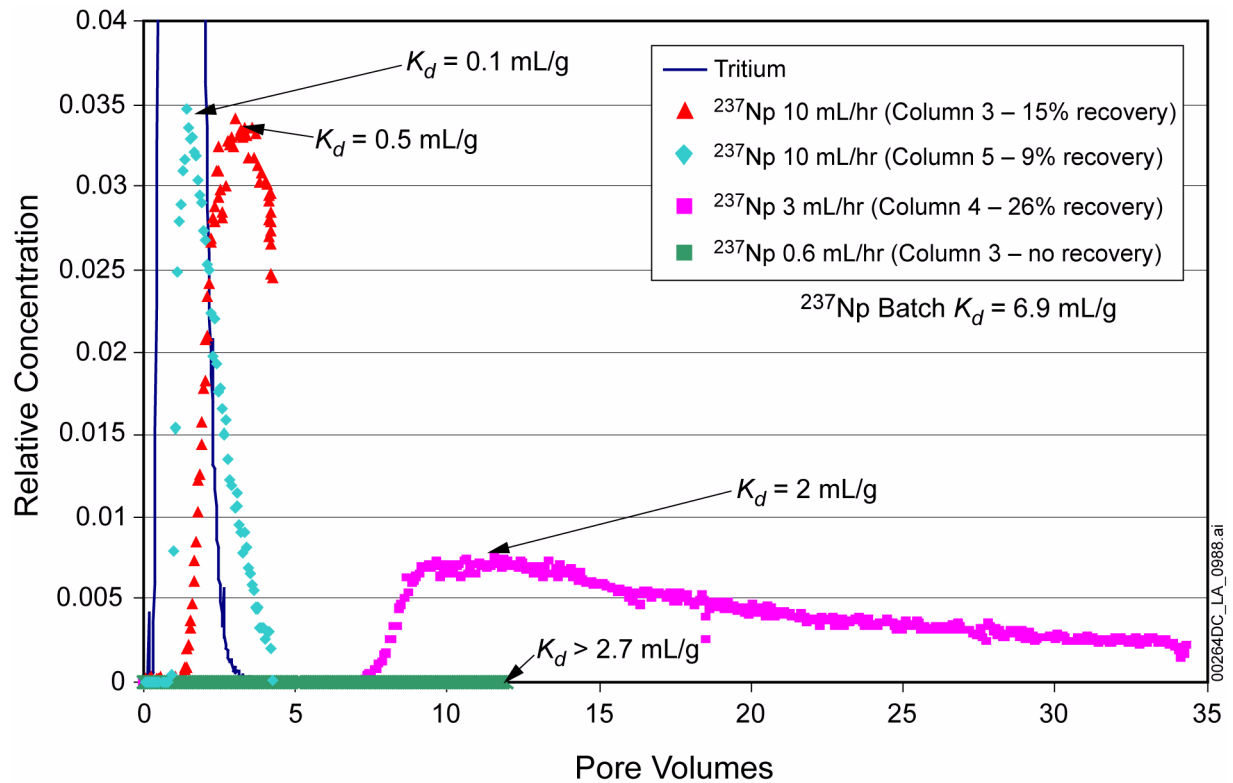
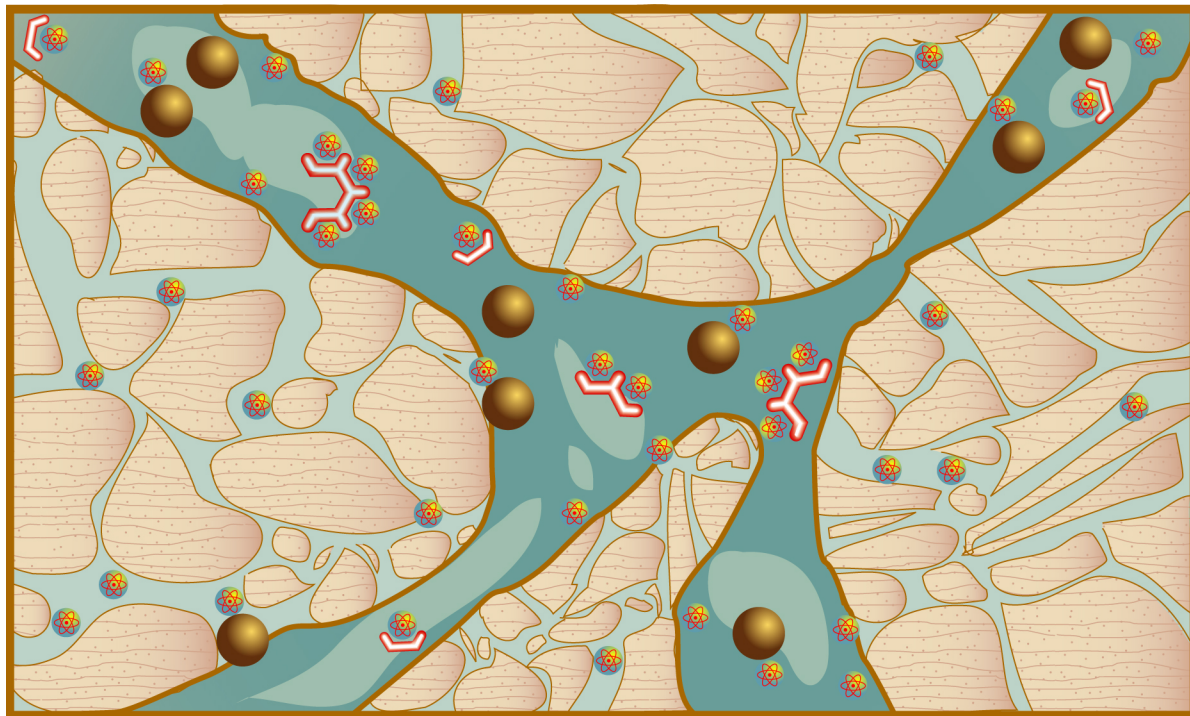


Figure 2.3.9-37. Breakthrough Curves and Recoveries of ^{237}Np in Laboratory Column Experiments Conducted at Three Flow Rates Using the Same Alluvium and Water

NOTE: Column 5 had a significantly higher hydraulic conductivity than column 3, and the tail of the breakthrough curve was truncated because of an artificially high background concentration (which was subtracted from the measured concentrations).

Source: SNL 2008a, Figure G-13.



00264DC_LA_0259.ai



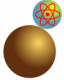

- | | | | |
|---|---|---|---|
|  | Radionuclide |  | Reversible Sorption Colloid Type Shown without Radionuclide Attached |
|  | Reversible Sorption Colloid Type Shown with Radionuclide Temporarily Attached |  | Irreversible Sorption Colloid Type Shown with Radionuclide Permanently Attached |

Figure 2.3.9-38. Schematic Showing Transport Processes Relevant to Colloid Transport in the Saturated Zone

Source: Adapted from SNL 2008b, Figure 6-2.

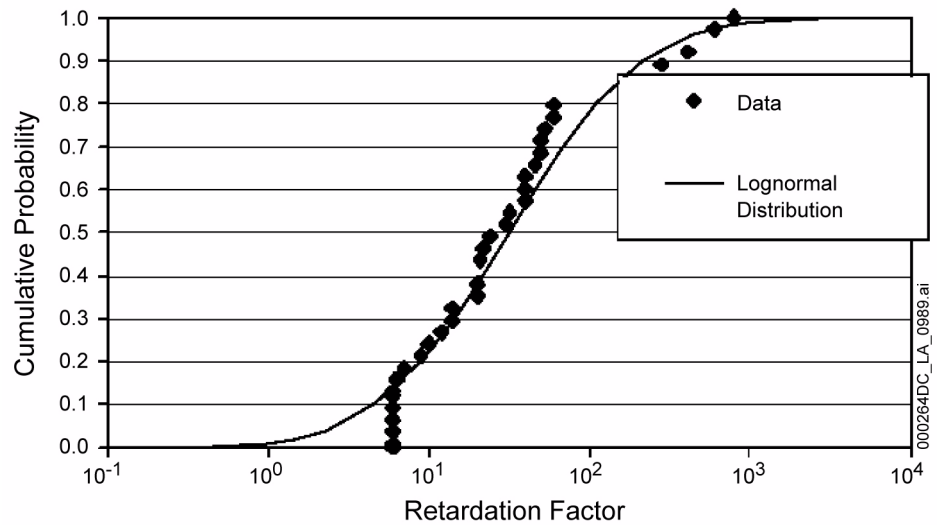


Figure 2.3.9-39. Cumulative Probability Distribution of the Log of the Colloid Retardation Factor and a Fit to the Data for Fractured Volcanic Rocks

Source: Adapted from BSC 2004e, Figure 6-3.

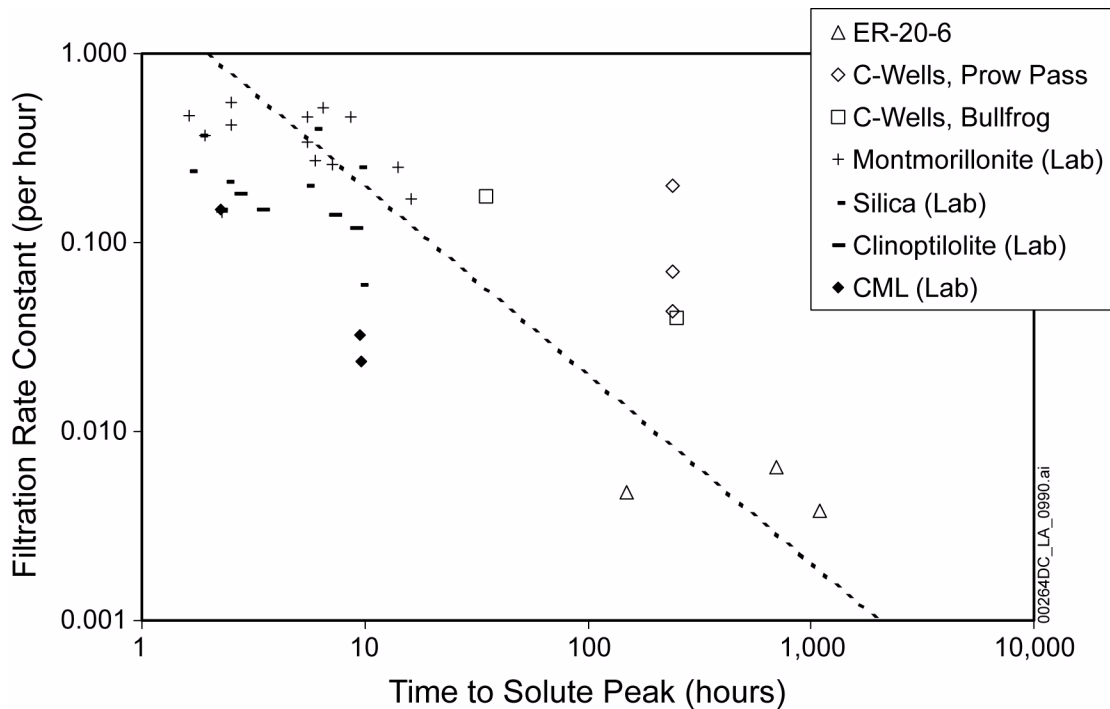


Figure 2.3.9-40. Carboxylate-Modified Polystyrene Latex Microsphere and Inorganic Colloid Filtration Rate Constants as a Function of Time to Solute Peak Concentration in Several Field and Laboratory Tracer Tests in Saturated Fractured Media

Source: BSC 2004e, Figure 6-1.

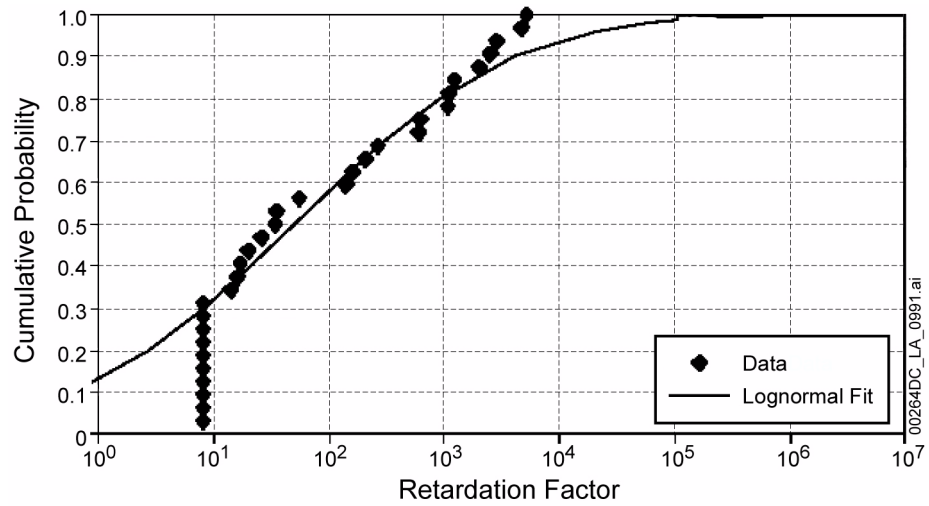


Figure 2.3.9-41. Cumulative Probability Distribution of Log of the Colloid Retardation Factor and a Fit to the Data for Alluvium Material

Source: Adapted from BSC 2004e, Figure 6-6; Viswanathan 2003, p. 24.

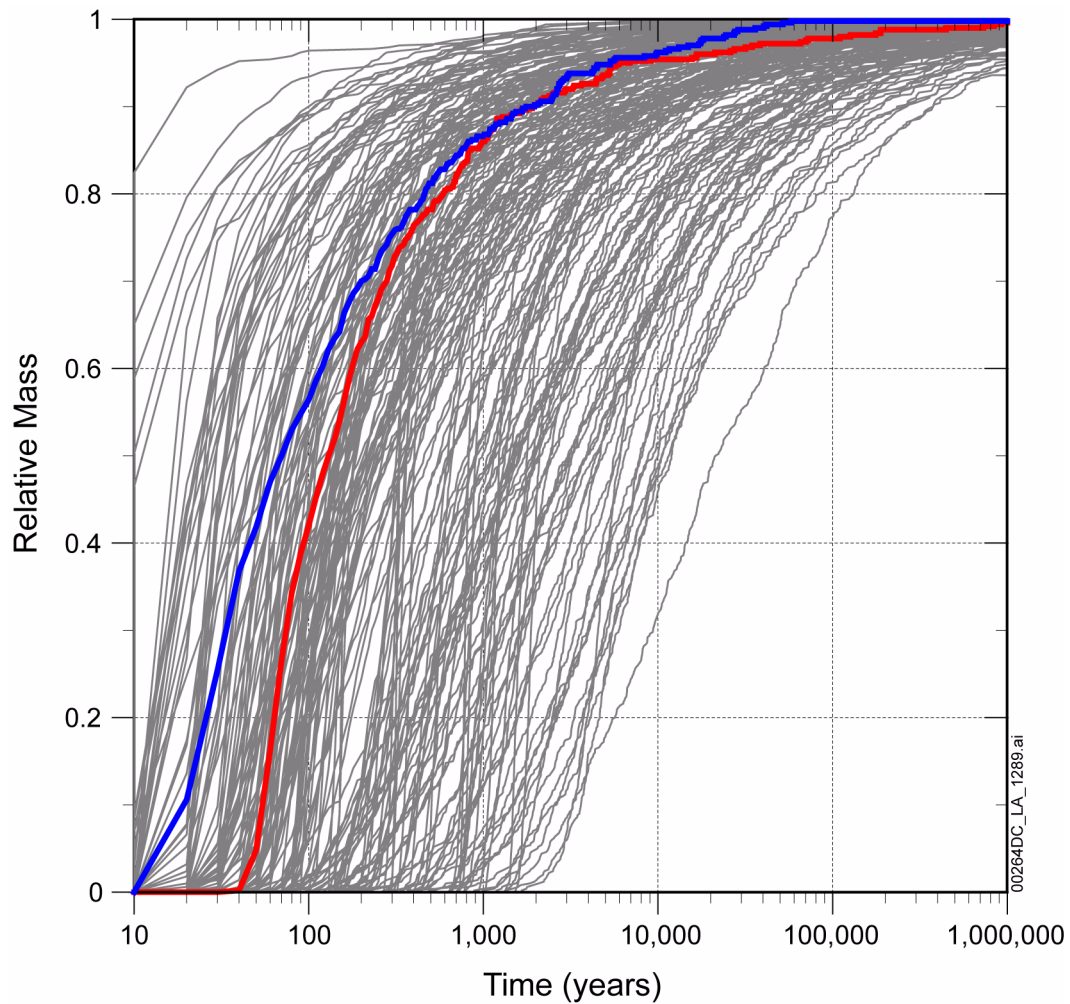


Figure 2.3.9-42. Simulated Mass Breakthrough Curves for the Median Case (Red Curve) and the High-Permeability-Zone Model (Blue Curve) for a Nonsorbing Radionuclide

NOTE: Breakthrough curves are for glacial-transition climatic conditions and do not include radioactive decay. Gray breakthrough curves are for the 200 realizations from the saturated zone flow and transport abstraction model of a nonsorbing radionuclide, as shown in [Figure 2.3.9-16](#).

Source: SNL 2008b, Figure 6-18[a].

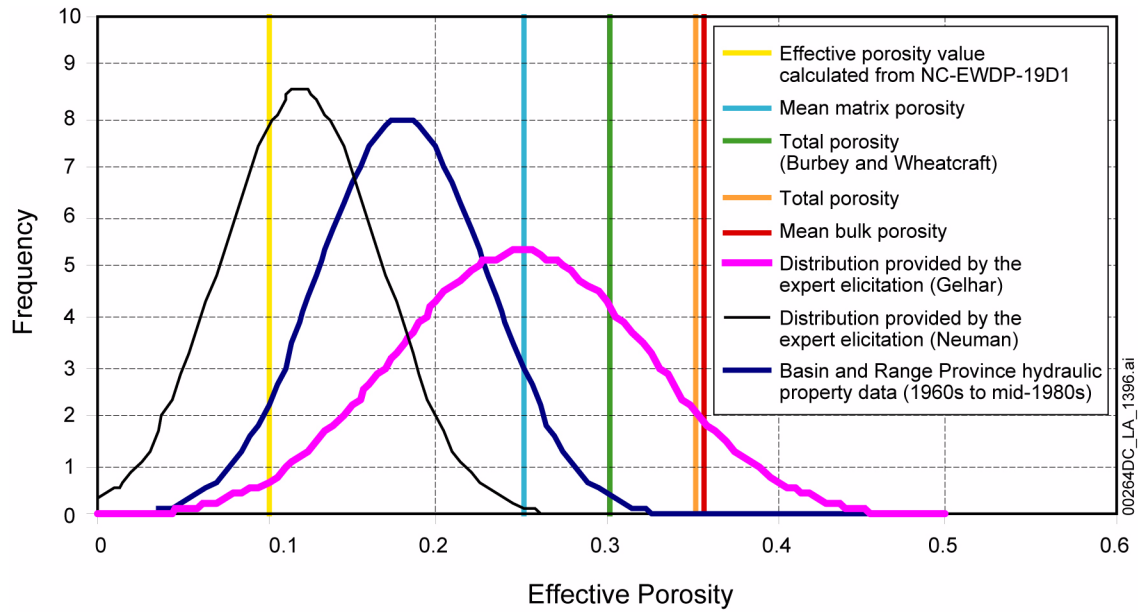


Figure 2.3.9-43. Range of Effective Porosities for Alluvial Materials

Source: SNL 2008b, Figure 6-9; Burbey and Wheatcraft 1986.

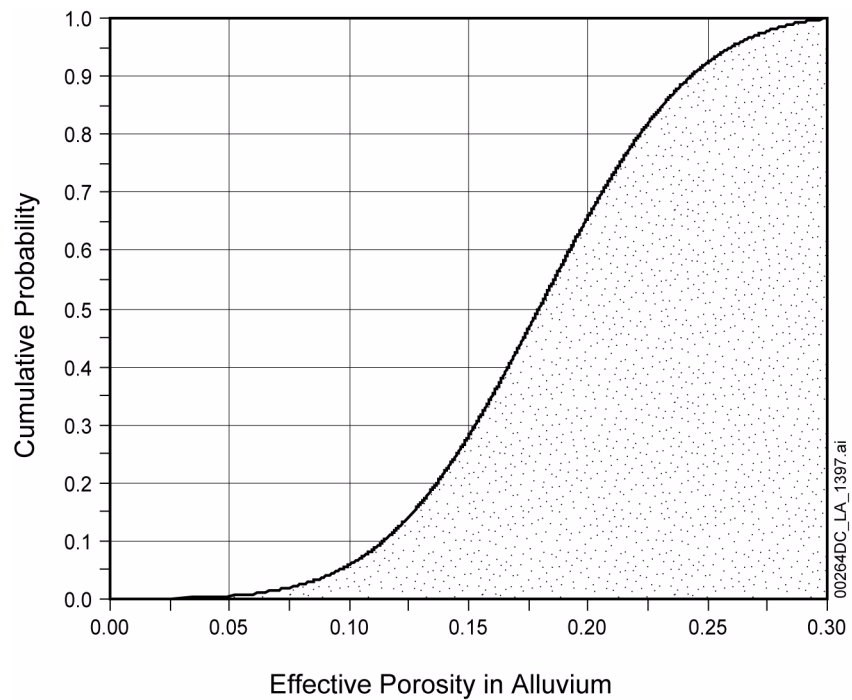


Figure 2.3.9-44. Effective Alluvium Porosity Distribution Used in Site-Scale Saturated Zone Transport Model

Source: SNL 2008b, Figure 6-10.

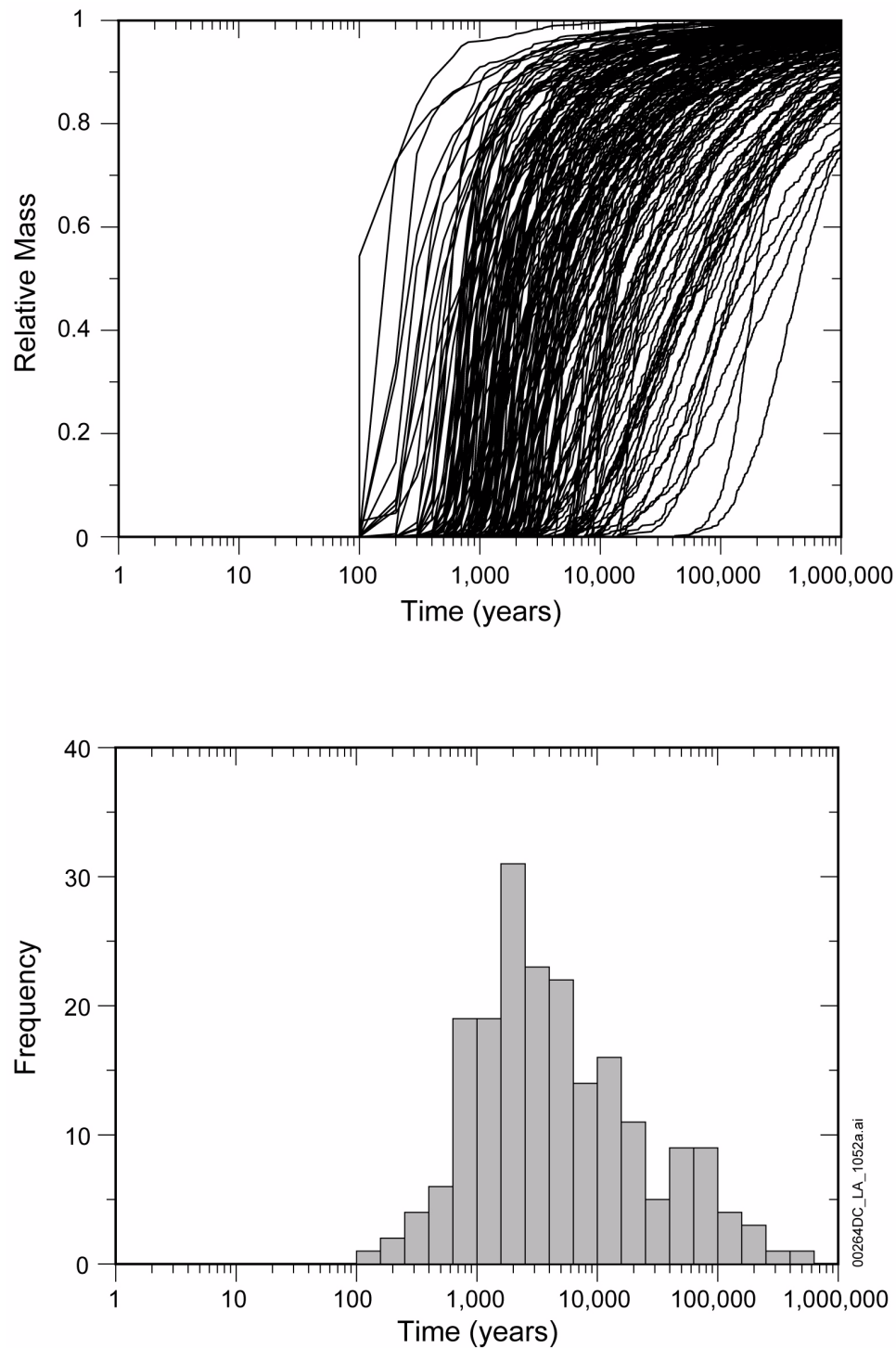


Figure 2.3.9-45. Mass Breakthrough Curves (Upper) and Median Transport Times (Lower) for Neptunium at the Accessible Environment for the Glacial-Transition Climate

NOTE: Mass breakthrough curves and median transport times are scaled for glacial-transition climate and do not include radionuclide decay. Results shown for 200 realizations from source region 1, below the northwestern part of the repository.

Source: SNL 2008b, Figure 6-11[a].

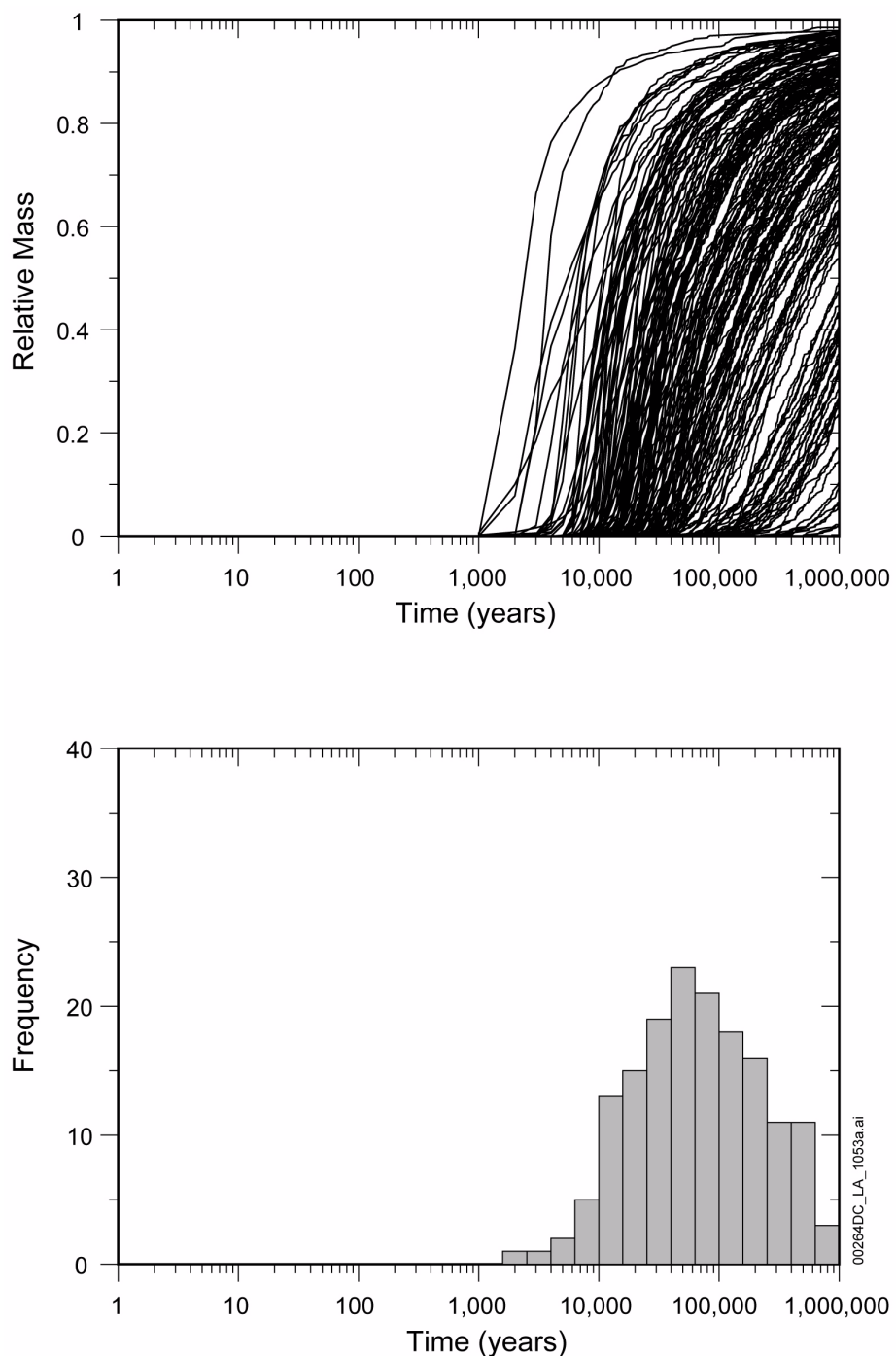


Figure 2.3.9-46. Mass Breakthrough Curves (Upper) and Median Transport Times (Lower) for Plutonium on Reversible Colloids at the Accessible Environment for the Glacial-Transition Climate

NOTE: Mass breakthrough curves and median transport times are scaled for glacial-transition climate and do not include radionuclide decay. Results shown for 200 realizations from source region 1. All plutonium mass, not transported as irreversibly attached to colloids in the saturated zone, is transported as reversibly attached to colloids.

Source: SNL 2008b, Figure 6-9[a].

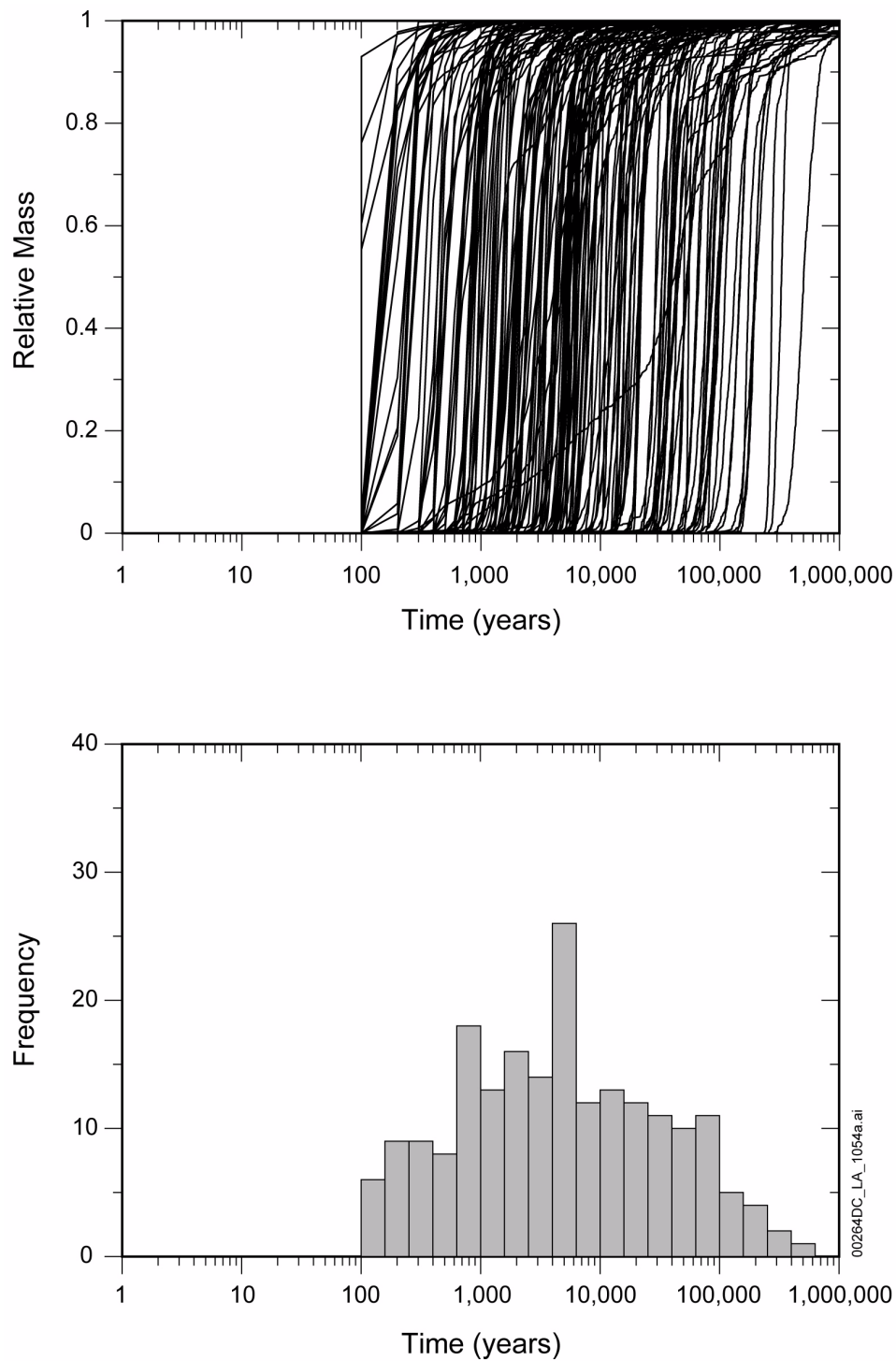


Figure 2.3.9-47. Mass Breakthrough Curves (Upper) and Median Transport Times (Lower) for Plutonium and Americium Irreversibly Attached to Colloids at the Accessible Environment for the Glacial-Transition Climate

NOTE: Mass breakthrough curves and median transport times are scaled for glacial-transition climate and do not include radionuclide decay. Results shown for 200 realizations from source region 1.

Source: SNL 2008b, Figure 6-12[a].

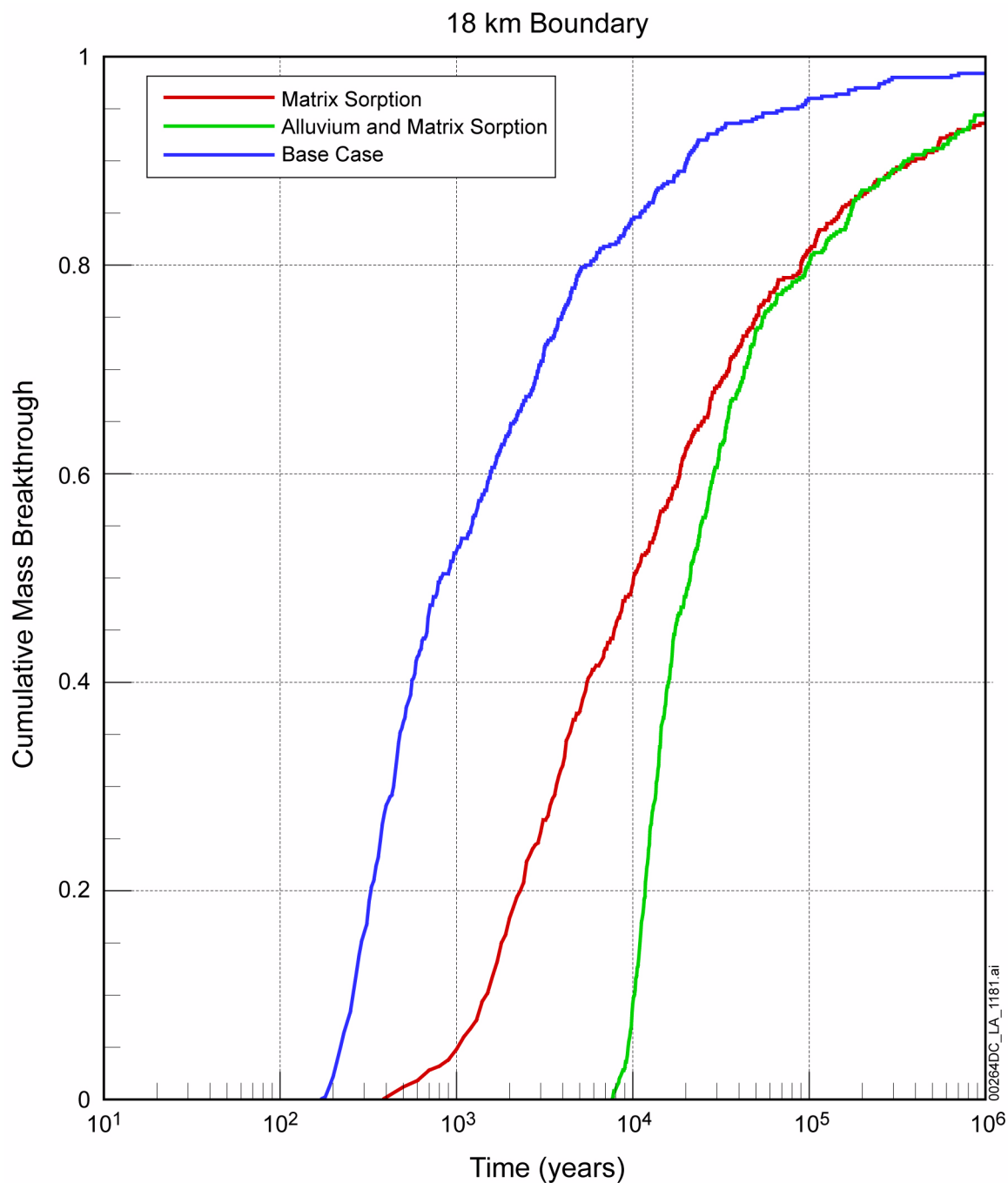


Figure 2.3.9-48. Comparison of Breakthrough Curves for Nonsorbing (Base Case) and Sorbing Cases Predicted by the Site-Scale Saturated Zone Transport Model at the Accessible Environment for Present-Day Climate

NOTE: Transport trajectories start in the saturated zone beneath the repository and end at the compliance point about 18 km south of the repository. Mass breakthrough curves and median transport times are for an instantaneous source and do not include radionuclide decay. For the sorbing cases, the sorption coefficient in the volcanic matrix is 1.3 mL/g and the sorption coefficient in the alluvium is 6.3 mL/g, corresponding to the median values from the uncertainty distributions for neptunium sorption (Table 2.3.9-4).

Source: SNL 2008a, Figure 6.8-1a.

INTENTIONALLY LEFT BLANK